Gas Contrasting of Multiphase and Composite Materials

E. Nold, G. Ondracek
Institut für Material- und Festkörperforschung

Kernforschungszentrum Karlsruhe

GAS CONTRASTING OF MULTIPHASE AND

COMPOSITE MATERIALS

E. Nold, G. Ondracek

Summary

The contrast between various constituents of multiphase materials is the most important factor for quantitative microstructural analysis. How to achieve it by gas contrasting is the subject of the present report, which starts in its first part with the description of the gas-contrasting chambers and the technique of gas contrasting, continues with the demonstrating and explanation of gas-contrasted metal, composite, and ceramic microstructures, and finishes with the interpretation of the gas-contrasting effect on the basis of the theory of thin interference layers.

In the second part the structure of an HfC-Co hard metals was gascontrasted for the purpose of quantitative microstructural analysis. Interference coatings were formed on the structural components in the process. These produce the desired colour contrast. Their structure is investigated using auger electron spectroscopy. It was found that, independent of the cathode material used, the coating overall contains mainly oxygen and the cathode element, that the oxygen concentration beyond a certain depth in the coating assumes approximately the value of uncoated specimen, that below this depth in the coating the cathode material can no longer be identified and that above this depth in the coating no hafnium or carbon is detectable on the HfC-phase while cobalt is present in the coating structure in the Co-phase.

5
THE GAS CONTRASTING METHOD

Dr. Gerhard Ondracek

University and Nuclear Center
Karlsruhe, FR Germany

It is essential to the qualitative and quantitative micro-scopic analysis of a material's microstructure that its con-stituents be distinguishable. Distinctions between the phases, crystallites, and boundaries of the polished section are based on their differential interaction behavior—re-flection and absorption—with optical light rays in optical microscopy or with electron beams in electron micros-copy. To obtain an image that can be analyzed microscop-ically—i.e., which is rich in contrast—these differences in the reflection or absorption behavior of the microstruc-tural constituents must be "intensified." The relevant methods of preparation are classed under the term, *con-trasting.* Especially in quantitative microstructural analy-sis, as schematically summarized in Fig. 5-1 this contrast-ing step is of particular importance.

The microstructural constituents in the microscopic image can be differentiated either by a bright/dark con-trast or by a color contrast. The bright/dark contrast is based on intensity differences of the light waves (ampli-tude condition); the color contrast, on differences in wave length (phase condition). Methods of contrasting are based either on the formation or removal of surface layers or on the simple use of optical aids. The use of optical aids (polarized, brightfield and darkground illumination, filters, etc.) is restricted, however, to certain properties of the specimens (e.g., polarizability of phases), but it has the advantage of keeping the surface of the specimen unchanged.[1,2]

The removal of surface layers—as, for example, by ca-thodic ion etching[3,4,5]—changes the polished surface but may bring out an even more "true image" of the micro-structure, since deformed surface parts disappear. On the
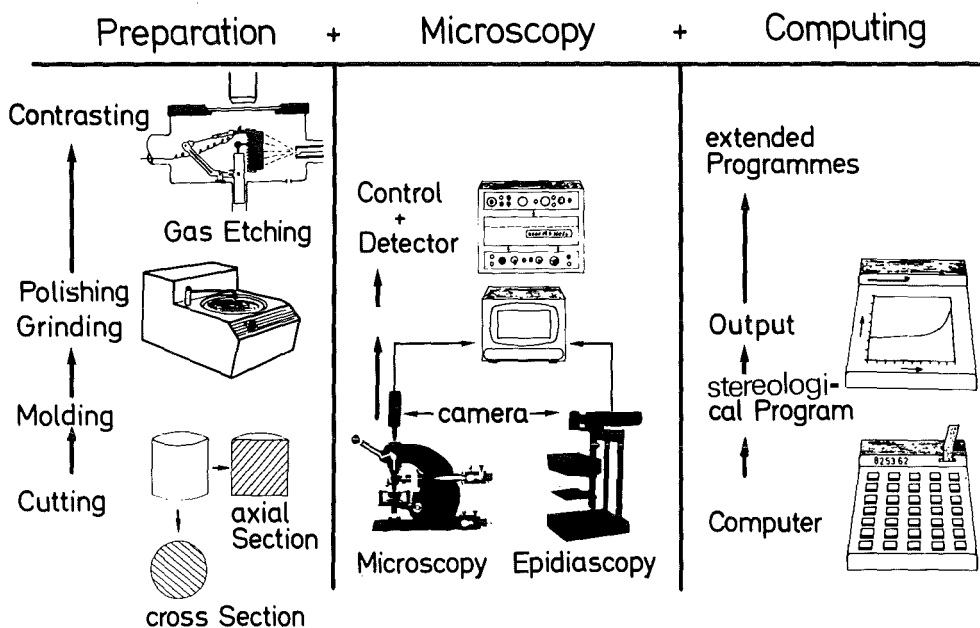

Fig. 5-1. Elements of Quantitative Microstructural Analysis (QMA).

other hand, however, the contrasting effect remains restricted. This is the reason why layer formation is usually the most effective way to contrast. Contrasting layers are produced either by vapor phase deposition,[6,7,8] where practically no interaction occurs between the layer and the sample surface, or by chemical or electrochemical etching. In the latter case, interaction between the etching agent and the polished section surface takes place.[9,10,11] Gas contrasting, as described in the next section, belongs to the layer forming methods.[12,13,14,15]

THE GAS-CONTRASTING APPARATUS

Gas contrasting takes place in a vacuum chamber that is externally similar to a hot stage attached to the mechanical stage of a microscope. The working principle is illustrated in Fig. 5-2[14,15]; the chamber, in Fig. 5-3 (see color insert). The sample is handled in one of three ways:

1. It is connected separately between two electrodes (cathode, anode).

2. It serves itself as anode if it is a conducting material.
3. It is directly fixed on the adjustable anode, which can be swiveled and therefore alternatively moved into the position opposite the cathode or below the microscope objective (see Fig. 5-2). Doing so permits the contrasting process to be controlled directly by tilting the specimen below the microscope objective for *in-situ* observation.

The gas-contrasting chamber prototype (Fig. 5-3) takes normal-sized, mounted metallographic specimens ($\sim$ 25 mm in diameter).[16,17] Its airtightness is increased by the pneumatic tilting device because the latter is operated by the same gas used for etching. Figure 5-2 illustrates its mode of operation. In the upper diagram, two needle valves (1 and 2) are shut and one (3) is open. This disposition sets up an excess pressure in the cylinder that moves the piston and lever system. The specimen is pneumatically tilted under the objective and automatically seated by resting against the cover glass. The piston stroke and,
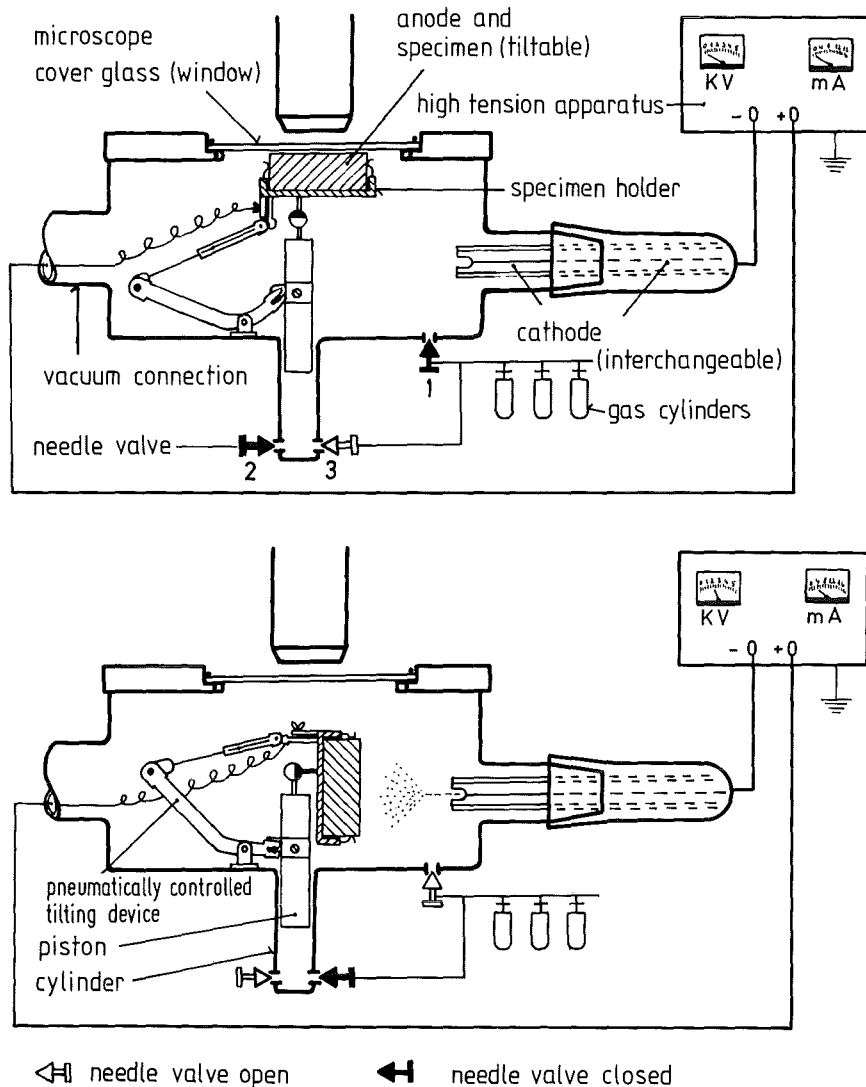

Fig. 5-2. The gas-contrasting chamber.

hence, the specimen height (11 to 15 mm) and diameter (< 27 mm) can be varied by means of adjusting screws. If the position of the valves is altered to correspond with the lower diagram in Fig. 5-2, the piston falls. Since the specimen with its holder is attached to the piston eccentrically through a ball joint, it tilts back under its own weight into a vertical position opposite the cathode.

THE PRINCIPLE OF GAS CONTRASTING

After the pumping unit connected to the pump nozzle is used to evacuate the gas-contrasting chamber, as shown in Fig. 5-2, it is filled via the needle valves with the etching gas or gas mixture. The ignited electron beam between the electrodes may be focussed by direct observation because the chamber (see Fig. 5-3) is transparent (it is made of quartz glass); the focussing additionally prevents discharging of the beam to chamber parts if they are nonconducting and different from the anode (quartz).

While the etching gas is being ionized by the electron beam, elements of the cathode material evaporate and mix into the gaseous etchant. The degree of ionization and evaporation—and with them, indirectly, the duration of contrasting—depends on the variable electrical data of current intensity and potential as well as on the distance between the sample anode and cathode and the gas pressure.[12] The gaseous ions may be produced either by accumulation of electrons on the neutral gas molecules— that is, by surface ionization (negative ions)[18]—or by impact ionization when accelerated electrons transfer their kinetic energy to neutral gas molecules via impact processes. In the latter case, positive ions are formed that are accelerated in the electrical field. They hit the cathode, causing sputtering of the cathode material.[19,20,21] The result is a mixture of atoms and/or ions of the etching gas and the cathode material; the mixture sublimates on the specimen's surface and forms interference layers that color different microstructural constituents differently. This effect is well known.[3]

Basically, no restriction exists with respect to various groups of materials for this type of layer formation. It takes place on the surfaces of the following:

1. Metallic materials, including intermetallic compounds
2. Composites, including hard metals
3. Ceramic materials, including glasses

The interaction tendency between the various materials and the etching gas is different, however, and this is why layer formation occurs in one of the following ways:

1. By interaction (reaction, solid solution) between the gaseous etchant and the material's constituents on the specimen's surface ("interaction layers")
2. By adsorption or sublimation of the gas atoms, ions, or molecules onto the material's constituents on the specimen's surface without interaction ("adsorption layers")

If the layer formation is based on interaction, it is controlled by the free energies of reaction or solution and their temperature dependencies, and these differ for the various microstructural constituents. In this case, differences in chemical composition and X-ray structure and differences in layer growth rate on the different microstructural constituents have to be taken into account. Interactions promote temperature increases in gas contrasting (Fig. 5-4).[14]

If the specimen is not directly connected to the anode, sublimation might be especially favored because heating of the specimen will not then occur, thereby promoting adsorption layer formation. Adsorption layers for all microstructural constituents should have approximately identical chemical composition, structure, and thickness because their growth rate is constant across the specimen surface.
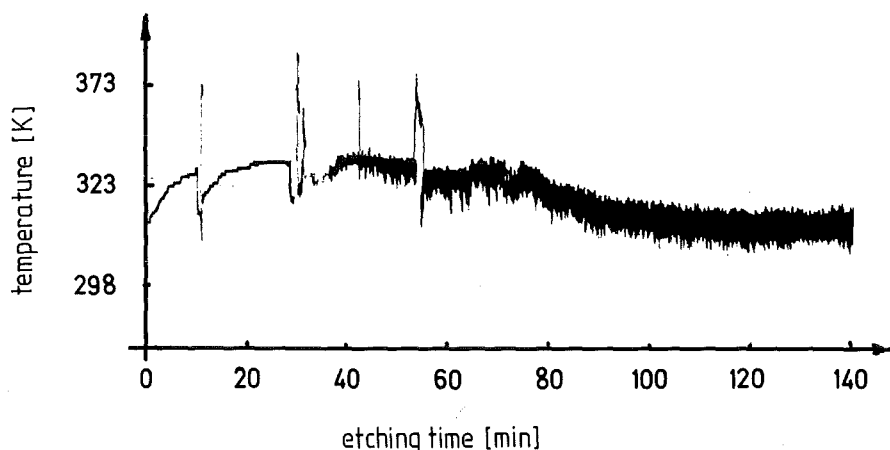

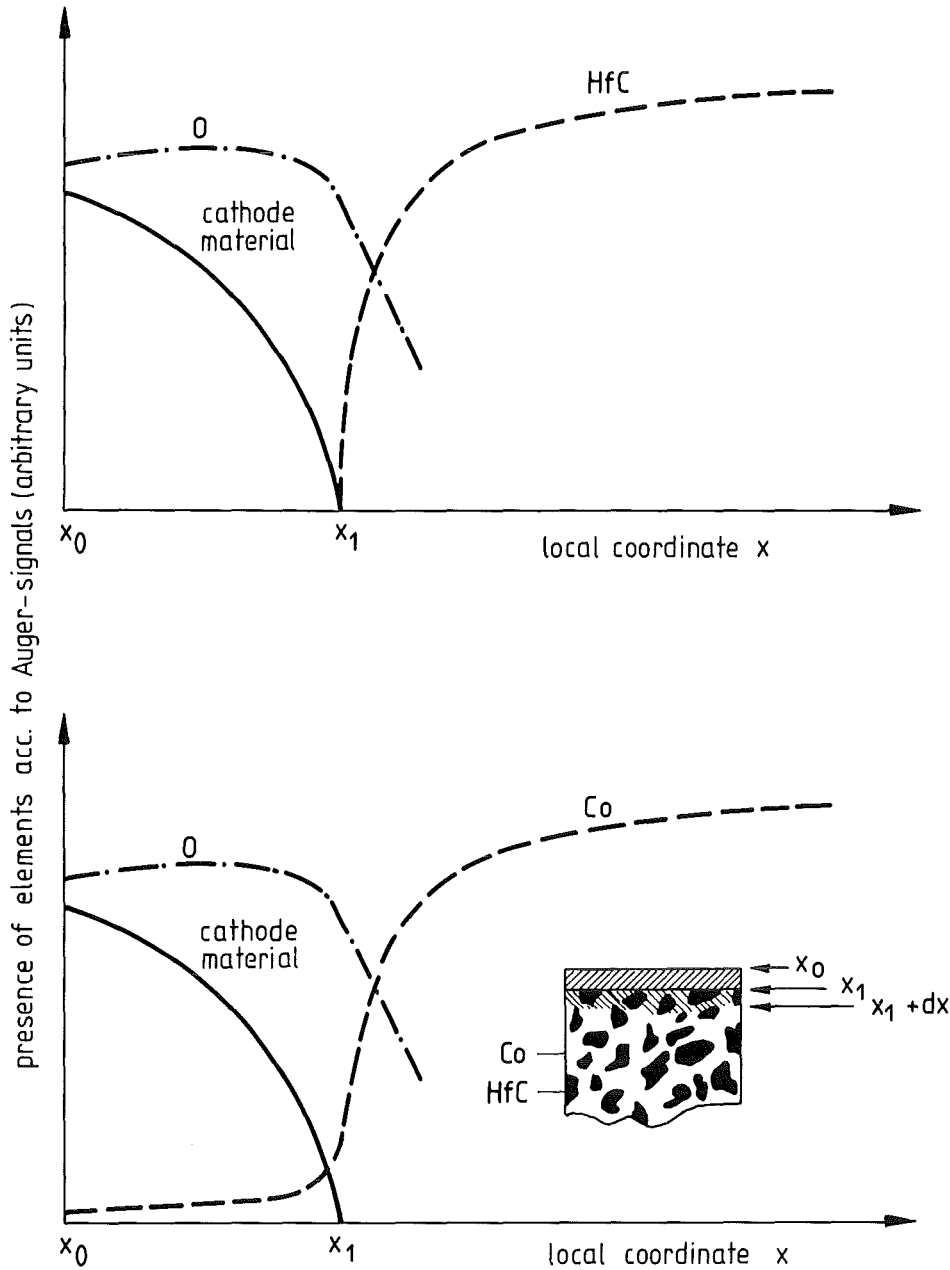Fig. 5-4. Surface temperatures during gas contrasting.

Fig. 5-5. Layer composition of gas-contrasted HfC-Co hard metal.

A study of gas-contrasted HfC–Co hard-metal microstructures using Auger electron spectroscopy[22] recently demonstrated the following:

1. A layer grows on the original, uncoated surface ("grown zone") that is predominantly formed by the elements of the gaseous etchant (etching gas and evaporated atoms from the cathode material).
2. Elements of the original specimen material may migrate into the growing layer, but this depends on the type of constituent.
3. Elements of the etching gas penetrate the interface between the layer and the original, uncoated surface, thereby altering its nature at least slightly ("diffusion zone").

Subsequently, a layer formed by gas contrasting is subdivided into, and is inhomogeneous within, two zones— a grown zone and a diffusion zone. The layer may be composed differently on different phases or constituents.

These results are summarized graphically and schematically in Fig. 5-5. Similar information about an inhomogeneous and nonstoichiometric layer structure was formerly obtained by Auger analysis of layers after chemical etching.[23]

GAS-CONTRASTED MICROSTRUCTURES

In order to get a more general assessment about gas contrasting, experiments have been performed with various classes of materials, as follows:

1. Single and multiphase metals, including intermetallic compounds
2. Composites, including hard metals
3. Ceramic materials

The microstructures of some of these have been selected to serve as examples. Others are shown in the quoted literature.

During the experiment for contrasting the polished structure of an austenitic steel by means of oxygen ions, a certain color sequence occurred with increasing contrasting time.[14] An improvement of the original contrast between crystallites and grain boundaries produced by chemical etching did not occur.

The same phenomenon occurs in the example shown in Fig. 5-6 of a two-phase infiltrated alloy of copper and tungsten. Figure 5-6(a) shows the polished microstructure as it appeared under the microscope. Chemical etching (10-percent aqueous ammonium-persulphate solution) leads to a negligible increase in the contrast differentiation between the two phases [Fig. 5-6(b)], which, however, is not comparable with the color contrast obtained by means of gas contrasting in oxygen [Figs. 5-6(c) and (d)]. In addition, this color contrast can be controlled with the contrasting duration. It is true that the same characteristic color sequence as in steel is produced for both phases, but the same color sequence occurs in copper after a different contrasting duration than that for tungsten. The color sequence is also present at the oxide inclusions [Figs. 5-6(c) and (d), blue]. (See color insert for Figs. 5-6 through 5-11.)

Differentiation of the phases is considerably improved by means of gas contrasting, but grain boundaries or crystallites do not become visible. Figure 5-7 shows intermetallic phases of uranium and silicon (U_3Si_2, U_3Si) together in one microstructure, where U_3Si is the matrix phase and U_3Si_2 are the discrete second-phase particles. As made clear by Fig. 5-7, gas contrasting provides definite contrast distinction between the phases. The bright and dark contrast distinction required for quantitative microstructural analysis may be easily obtained by use of color filters.[24] All phases again traverse (after differential contrasting time) the characteristic color sequence as in the other examples, finally entering an achromatic state that is no longer subject to change.

Hard metals form an important group among composites, for which gas contrasting usually provides satisfying contrast. Figure 5-8 illustrates the microstructure of HfC–Co hard metal, which was the subject for the investigation of the layer structure (see Fig. 5-5). As demonstrated in Fig. 5-9, both phases—the metal binder as well as the carbide phase—traverse the characteristic color sequence but shift mutually in time. This statement also holds true for oxide cermets (Fig. 5-10) as well as single-phase ceramics (Fig. 5-11), where the complete color sequence occurs slower than it does in metals. The results of these experiments can be summarized as follows:

1. Gas contrasting produces a characteristic color sequence with increasing contrasting duration, and this is independent of the material, the structure, the type of gas, and other contrasting conditions.
2. The colors assumed by the various phases or constituents of a microstructure after a certain duration of contrasting under otherwise identical conditions differ; i.e., the relative speed with which the various constituents traverse the characteristic color sequence depends on the material.
3. For "two-dimensional" features, such as grain or phase boundaries, gas contrasting does not provide contrast improvement.
4. The absolute speed of sequence of the colors depends on the etching conditions such as the type and pressure of gas, intensity and potential of current, and distance between electrodes.
5. The color sequence always ends in an achromatic, unchangeable state.
6. The relatively different speed of the color sequence in various constituents permits their contrasting through reproducible and controlled color contrast.
7. For the purpose of quantitative microstructural analysis, the color contrast may be converted into bright-dark contrast by using interference filters at the microscope.

THE INTERPRETATION OF THE GAS-CONTRASTING EFFECT

As mentioned at the beginning of this Chapter, it is a necessary presupposition for the optical differentiation and quantitative microscopical description that sufficient contrast exist between the various constituents of a microstructure. Bright-dark contrast is mathematically defined to be

$$K = \frac{R_\alpha - R_\beta}{R_\alpha} \qquad (5\text{-}1)$$

where reflectance is defined as the ratio between reflected and incident (original) radiation intensity, and the reflection coefficient, r (see Eqs. 5-2, 5-3, and 5-4), is defined by the root of the reflectance, R ($r_\alpha = \sqrt{R_\alpha}$; $r_\beta = \sqrt{R_\beta}$). R_α and R_β are the reflectances of constituents α and β, respectively.

With the limiting condition,

$$R_\alpha > R_\beta$$

Eq. 5-1 establishes the following:

$$0 \leq K \leq 1$$

Maximum bright-dark contrast is obtained with minimum reflectance of microstructural constituent β, or

$$K \rightarrow K_{max} \quad \text{for} \quad R_\beta \rightarrow R_{min}$$

or

$$\lim_{R_\beta \rightarrow 0} K = 1$$

Taking into account that contrast enhancement by gas contrasting is based on layer formation, the theoretical consideration has to start with the reflectance of the "coated" constituent β, that is, $R_{\beta S}$, which, according to the Fresnel equation for normal incidence, has the form[7,25,26,27]

$$R_{\beta S} = \frac{r_0{}^2 + r_1{}^2 + 2\,r_0 r_1 \cos \Delta\lambda}{1 + r_0{}^2 r_1{}^2 + 2\,r_0 r_1 \cos \Delta\lambda} \qquad (5\text{-}2)$$

where $r_0\ (=\sqrt{R_0})$, the reflection coefficient at the interface environment/layer, is defined as follows:

$$r_0 = \sqrt{\frac{(n_S - n_O)^2 + k_S{}^2}{(n_S + n_O)^2 + k_S{}^2}} \qquad (5\text{-}3)$$

and $r_1\ (=\sqrt{R_1})$ the reflection coefficient at the interface layer/constituent, as:

$$r_1 = e^{-\left(\frac{4\pi k_S}{\lambda}\right)d_S} \sqrt{\frac{(n_\beta - n_S)^2 + (k_\beta - k_S)^2}{(n_\beta + n_S)^2 + (k_\beta + k_S)^2}} \qquad (5\text{-}4)$$

and the optical phase shift between incident and reflected beam, $\Delta\lambda$, as

$$\Delta\lambda = \left(\frac{4\pi n_S}{\lambda}\right)d_S + \delta_{OS} - \delta_{S\beta} \qquad (5\text{-}5)$$

In Eqs. 5-3, 5-4, and 5-5,

$n_O,\ n_S,\ n_\beta$ = refractive index of environment (O), layer (S), and constituent (β), respectively

$k_O,\ k_S,\ k_\beta$ = absorption coefficient of environment (O), layer (S), and constituent (β), respectively

λ = wavelength of optical beam

d_S = layer thickness on constituent β of microstructure

The first term, $\left(\dfrac{4\pi n_S}{\lambda}\right)d_S$, in Eq. 5-5 refers to the optical path difference between the incident and reflected light ray transformed into arc units, $\dfrac{2\pi}{\lambda}$, that results from the optical path through the interference layer, $2n_S d_S$, whereas the second, δ_{OS}, and the third, $\delta_{S\beta}$, terms describe the optical phase shiftings as transient conditions for the reflections at the interfaces of environment/layer and layer/constituent, respectively.[25]

In air or vacuum ($n_O = 1$); transmissive, nonabsorbing

layers [$n_O < n_S < n_\beta$; $k_S = 0$; $r \neq f\,(d_S,\ \lambda)$]; and almost nonabsorbing microstructural constituents ($k_\beta = 0$),[25] the optical phase shifts become

$$\delta_{OS} = \pi \qquad (5\text{-}6)$$

$$\delta_{S\beta} = \pi$$

and Eq. 5-5 becomes

$$\Delta\lambda = \left(\frac{4\pi n_S}{\lambda}\right)d_S + \pi - \pi \qquad (5\text{-}7)$$

Additionally, we observe that extinction interference on constituent β occurs if the optical phase shift for the beam becomes

$$\Delta\lambda = (2m + 1)\pi \qquad (5\text{-}8)$$

where $m = 0, 1, 2. \ . \ . \ .$

From Eq. 5-2, one obtains

$$R_{min} = \left[\frac{r_0 - r_1}{1 - r_0 r_1}\right]^2 \qquad (5\text{-}9)$$

and from Eq. 5-7,

$$d_S = \frac{(2m + 1)\lambda}{4n_S} \qquad (5\text{-}10)$$

Equation 5-10 is the well-known condition for optical interference extinction. Both Eqs. 5-9 and 5-10 provide the crucial basis for interpreting gas contrasting; that is, maximum bright-dark contrast is either (1) due to the fitting of the optical constants of the layer (n_S and k_S) and of the microstructural constituent β (n_β and k_β) in such a way that for *nonabsorbing* layers and independently of layer thickness, Eq. 5-9 results in the value, $R_{min} = 0$; or (2) takes place independently of the optical constants of the microstructural constituent β and with a definite layer thickness, d_S, on this constituent, in which case, with monochromatic light, λ, and given refraction index n_S, of the *nonabsorbing* layer material, Eq. 5-10 is fulfilled.

Microscopical microstructural analyses are usually made with white light, which is not monochromatic. Although differently reflected from various "uncoated" microstructural constituents, white light does not provide sufficient contrast [Fig. 5-12(a)]. After layer formation, however, a defined spectral color will suffer extinction by reflection according to Eq. 5-9 or 5-10; the color is different for different constituents. The rest of the spectral colors mix, resulting in nonwhite complementary colors, obviously different for the various constituents and therefore providing color contrast [Figs. 5-12(b) and (c)].
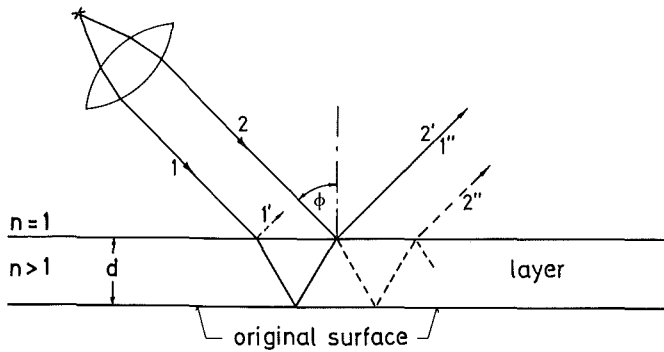
Fig. 5-13.   Reflection of monochromatic light on a coated surface (principle of thin-layer interference).

First, assuming that the growing layer on the various microstructural constituents achieves equal *thickness* whether or not identical *structure* [Fig. 5-12(b)], contrast—including color contrast—may occur as a result of the different interaction between the optical constants of the constituents and those of the layer (Eq. 5-9).

Second, assuming that the growing layer on the various microstructural constituents achieves identical or nonidentical structure but *unequal* thickness [Fig. 5-12(c)], contrast and color contrast follow from Eq. 5-10 even when the role of the optical constants of the constituents is neglected. (See color insert for Fig. 5-12.)

The existing results are inadequate to determine which mechanism controls gas contrasting or to what extent different mechanisms take part in it. To explain the gas-contrasting effect using an engineering approach, the following consideration must be restricted to a model with different layer thicknesses. This simplification does not state that the effect of the optical constants of the various microstructural constituents on contrasting may be generally neglected. In Fig. 5-13, a gas-contrasted specimen is imagined to be covered by nonabsorbing, transmissive layers of different thicknesses on different constituents. The light rays (1 and 2) coming from the objective are partially reflected from (1′ and 2′) and partially transmitted through the layer. The ray penetrating the layer changes its direction corresponding to the refractive index (n_S) of the layer. Ray 1, for example, is reflected again at the interface layer/constituent β and returns in the form of ray 1″ to the environment. There it interferes with the primarily reflected part 2′ of the original ray 2. Extinction occurs under the following condition:[28]

$$d_S = \frac{(2m + 1)\lambda}{4\sqrt{n_S^2 - \sin^2 \phi}} \qquad (5\text{-}11)$$

This equation leads to Eq. 5-10 in the case of normal beam incidence ($\phi = 0$). If the etched specimens are observed in white light, spectral colors satisfying the conditions in Eqs. 5-1 or 5-2 will suffer extinction. The remaining colors are superimposed to produce complementary or mixed colors. Since layer thickness is continually in-

creasing during gas contrasting, it reaches the value (480/2 nm) at which extinction occurs for the blue component of white light first. The corresponding complementary color can be obtained from the color triangle in Fig. 5-14 by drawing a straight line from the wavelength that has suffered extinction through the white point (W). The intersection of this straight line with the opposing side of the triangle gives the wavelength of the mixed color, which can then be compared on the color ring. If, for example, blue suffers extinction, the complementary color, yellow, is obtained. The white point for daylight (E) is displaced for artificial illumination according to the type of source (points A, B, and C in Fig. 5-14). As spectral colors of longer wavelength suffer extinction, the intersection point moves to the uncalibrated side of the triangle, the so-called *purple line*. It represents the purple tones that are not spectral colors themselves but a mixture of red and violet. (See color insert for Fig. 5-14.)

The characteristic color sequence during gas contrasting can be read off from the color chart. If the layer begins to form, the short wave colors interfere. Thus, the color sequence begins with yellow and traverses the colors shown on the color ring as they appear during gas contrasting. It must be taken into account that certain large layer thicknesses satisfy the condition for the destructive interference of certain colors but simultaneously satisfy the condition for the constructive interference of others,[7] as follows:

$$d = \frac{(m + 1)\lambda}{2\sqrt{n_S^2 - \sin^2\phi}} \qquad (5\text{-}12)$$

or for normal incidence,

$$d = \frac{(m + 1)\lambda}{2n_S} \qquad (5\text{-}13)$$

where $m = 0, 1, 2, 3. \ldots$. These colors make a reinforced contribution to the mixed color. When the layer thickness is considerably greater than the wave-length, the interference condition can be satisfied for several wavelengths simultaneously with the result that, as the color sequence is repeated over and over again, the colors in the sequence become modified. When the layer thickness is finally so great that light of all colors suffers extinction or reinforcement, the coloration fades because the total reflected light combines to colorless. The different phases then appear correspondingly colorless.

SUMMARY

The contrast between various constituents of multiphase materials is the most important factor for quantitative microstructural analysis. How to achieve it by gas contrasting is the subject of the present chapter, which starts with the description of the gas-contrasting chambers and

the technique of gas contrasting, continues with the demonstration and explanation of gas-contrasted metal, composite, and ceramic microstructures, and finishes with the interpretation of the gas-contrasting effect on the basis of the theory of thin interference layers.

REFERENCES

1. Petzow, G., and Knosp, H. *Handbuch der Mikroskopie in der Technik,* III–2, p. 27. Frankfurt-Main: Umschau-Verlag, 1969.
2. Rinne, F., and Berek, M. *Anleitung zu optischen Untersuchungen mit dem Polarisationsmikroskop,* p. 71. Stuttgart: Schweizerbart'sche Verlagsbuchhandlung, 1953.
3. Hilbert, F. *Neue Hütte* 6:368 (1962); 7:416 (1962).
4. Rexer, J., and Vogel, M. *Prakt. Metallographie* 5:361–368 (1968).
5. Schwaab, P. Z. *Metallkunde* 55:199 (1965).
6. Bühler, H. E., and Jäckel, G. Tafeln zur quantitativen Metallographie mit aufgedampften Interferenzschichten. *Arch. Eisenhüttenwesen* 41–9:859 (1970).
7. Pepperhoff, W., and Ettwig, H. H. *Interferenzschichten-Mikroskopie.* Darmstadt: Dr. Dietrich Steinkopff-Verlag, 1970.
8. Pepperhoff, W., and Schwab, P. *Handbuch der Mikroskopie in der Technik,* Bd. 3, Teil 2, p. 65. Frankfurt/Main: Umschau Verlag, 1969.
9. Petzow, G. *Metallographisches Ätzen* 5. Auflage, Berlin-Stuttgart: Gebrüder Borntraeger, 1976.
10. Petzow, G., and Exner, E. *Handbuch der Mikroskopie in der Technik,* III–1, p. 37. Frankfurt: Umschau-Verlag, 1968.
11. Weck, E., and Leistner, E. Metallographic instructions for color etching by immersion, p. 77 Deutscher Verlag für Schweißtechnik, 1970.
12. Bartz, G. *Prakt. Metallographie* X–5: 311 (1973).
13. Bartz, G. German Patent DP 2130605 (1973).
14. Ondracek, G., and Spieler, K. *Prakt. Metallographie* 6:324 (1973).
15. Ondracek, G., and Spieler, K. *Leitz-Mitt. Wiss. u. Techn.* VI–6:224 (1976).
16. Ondracek, G., and Spieler, K. German Patent DP 2433690 (1983).
17. Spieler, K. German Patent DP 2313801 (1973).
18. Westphal, W. *Kleines Lehrbuch der Physik,* p. 129. Berlin-Göttingen-Heidelberg: Springer-Verlag, 1948.
19. Flügge, S., and Trendelenburg, F. Ergebnisse der exakten Naturwissen-schaften, Bd. 35. Berlin: Springer-Verlag, 1964.
20. Hass, G. *Physics of Thin Films.* Vol. 3. New York: Academic Press, 1966.
21. Kohlrausch, M. *Prakt. Physik,* Bd. 2. Stuttgart: Verlag B. G. Teubner, 1962.
22. Nold, E., and Ondracek, G. *Prakt. Metallographie* 23:8 (1986).
23. Gahm, H.; Jeglitsch, F.; Hörl, E. M. *Prakt. Metallographie* 19:369 (1982).
24. Nazare, S., and Ondracek, G. *Prakt. Metallographie* 6:742 (1969).
25. Bergmann, L., and Schaefer, C. *Lehrbuch der Experimentalphysik,* Bd. III–Optik. Berlin-New York: Walter de Gruyter, 1974.
26. Heavens, O. S. *Optical properties of thin solid films.* New York: Dover Publications, 1965.
27. Vasicek, A. *Optics of Thin Films.* Amsterdam: North Holland Publ. Co., 1960.
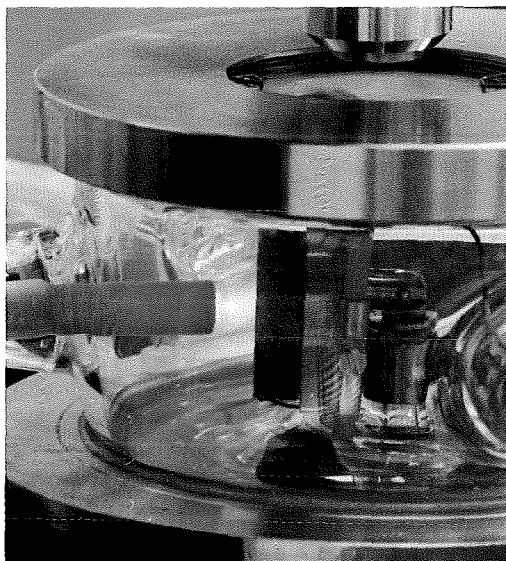28. Gerthsen, C. *Physik.* Berlin-Göttingen-Heidelberg: Springer-Verlag, p. 383, 1956.

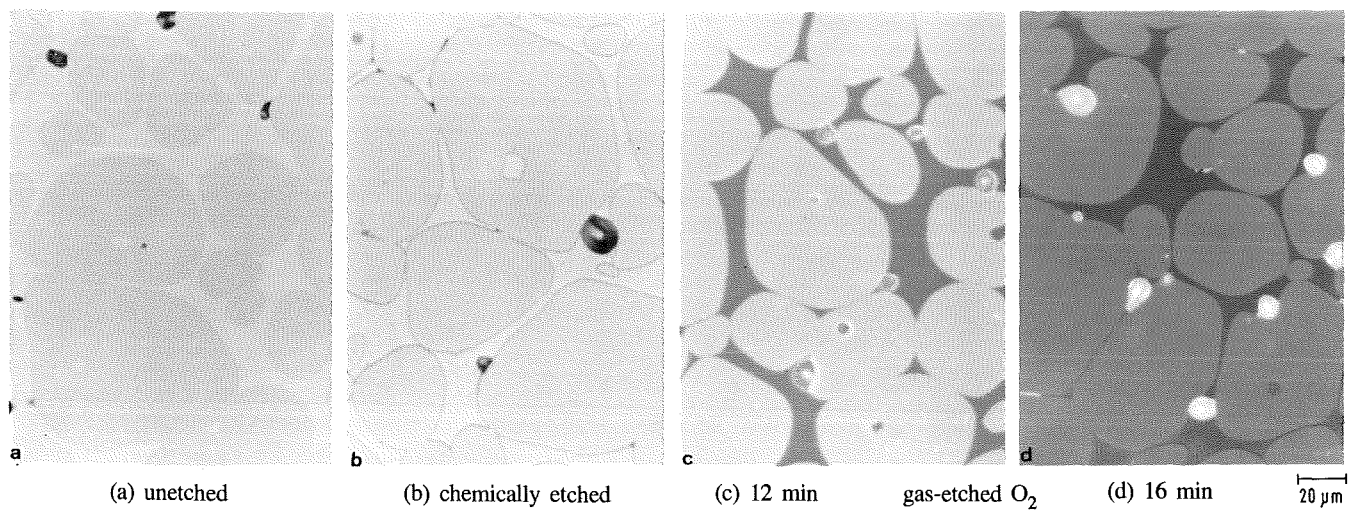Fig. 5-3. Gas-contrasting chamber on microscopic cross stage (in action).

(a) unetched   (b) chemically etched   (c) 12 min   gas-etched O_2 (d) 16 min   20 µm

Fig. 5-6. Gas-contrasted Cu–W infiltration alloy (for example: Cu = violet, W = orange; oxide = blue)
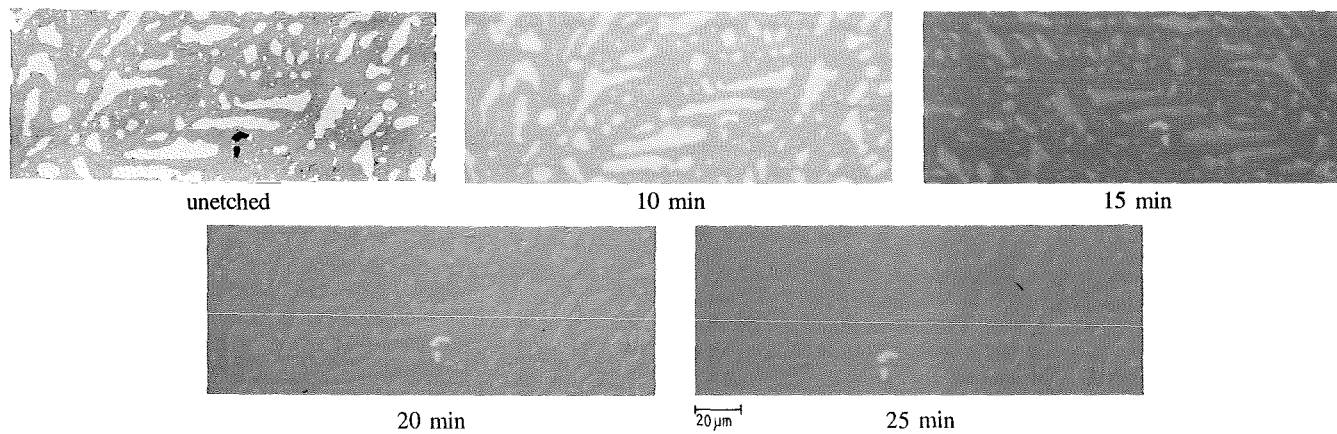

unetched   10 min   15 min

20 min   20µm   25 min

Fig. 5-7. Gas-contrasted U_3Si_2–U_3Si intermetallic two-phase material: U_3Si is the matrix phase and U_3Si_2 is the included phase (oxygen as contrasting gas; steel cathode; 1.05kV).
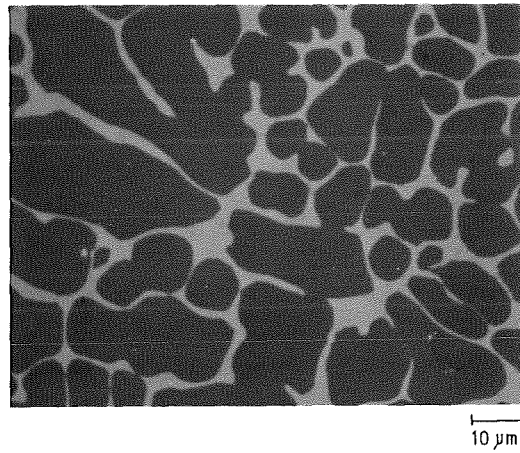
Fig. 5-8. Gas-contrasted HfC-Co hard metal (HfC = brown; Co matrix phase = gold).

| unetched | 5 min | 10 min |

| 15 min | 20 min | 25 min |
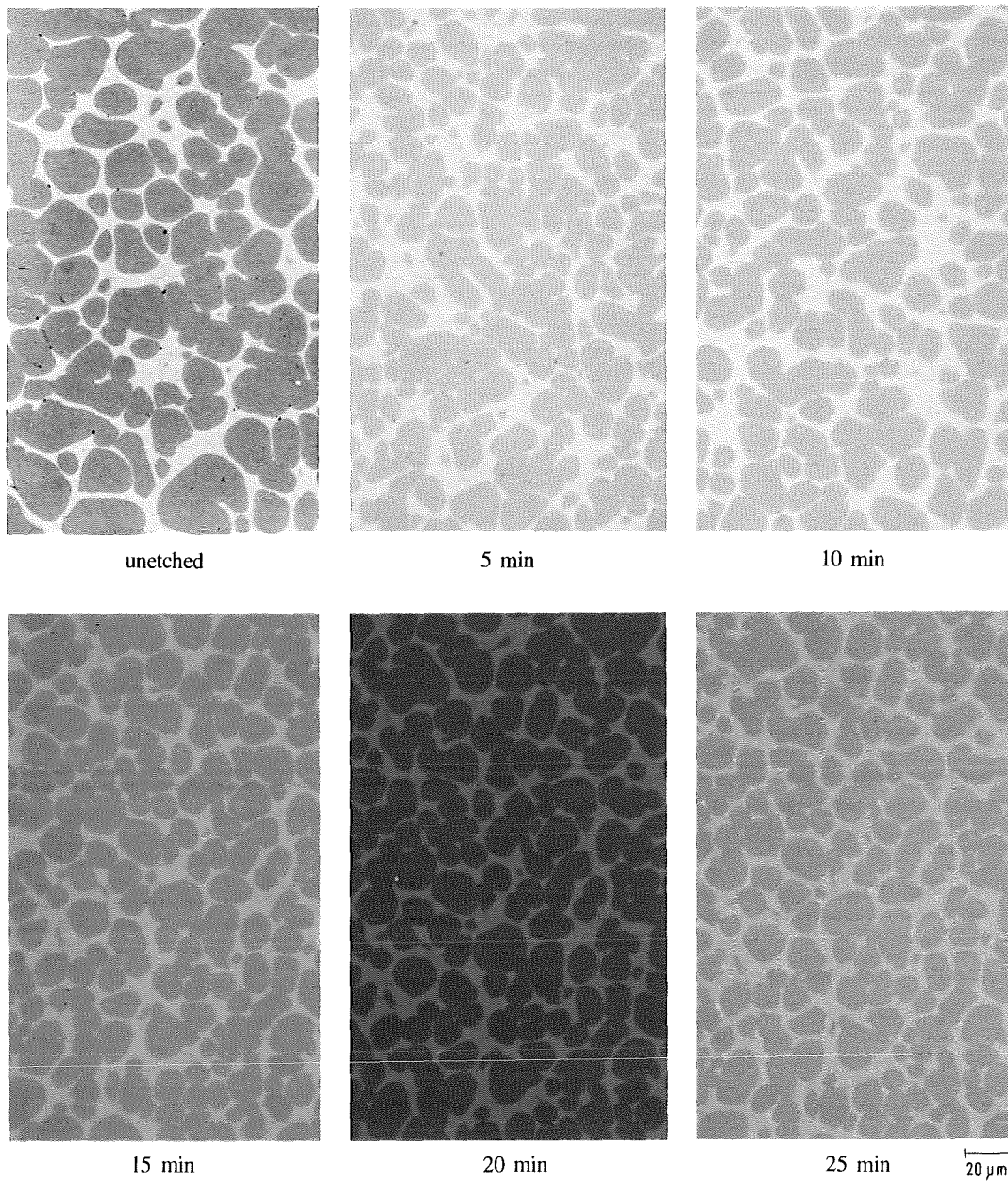
Fig. 5-9. Color sequence in HfC–Co hard metal by gas contrasting (oxygen as contrasting gas; steel cathode; 1.05kV).

unetched   5 min   10 min

15 min   20 min   25 min

30 min   35 min   40 min   20 µm
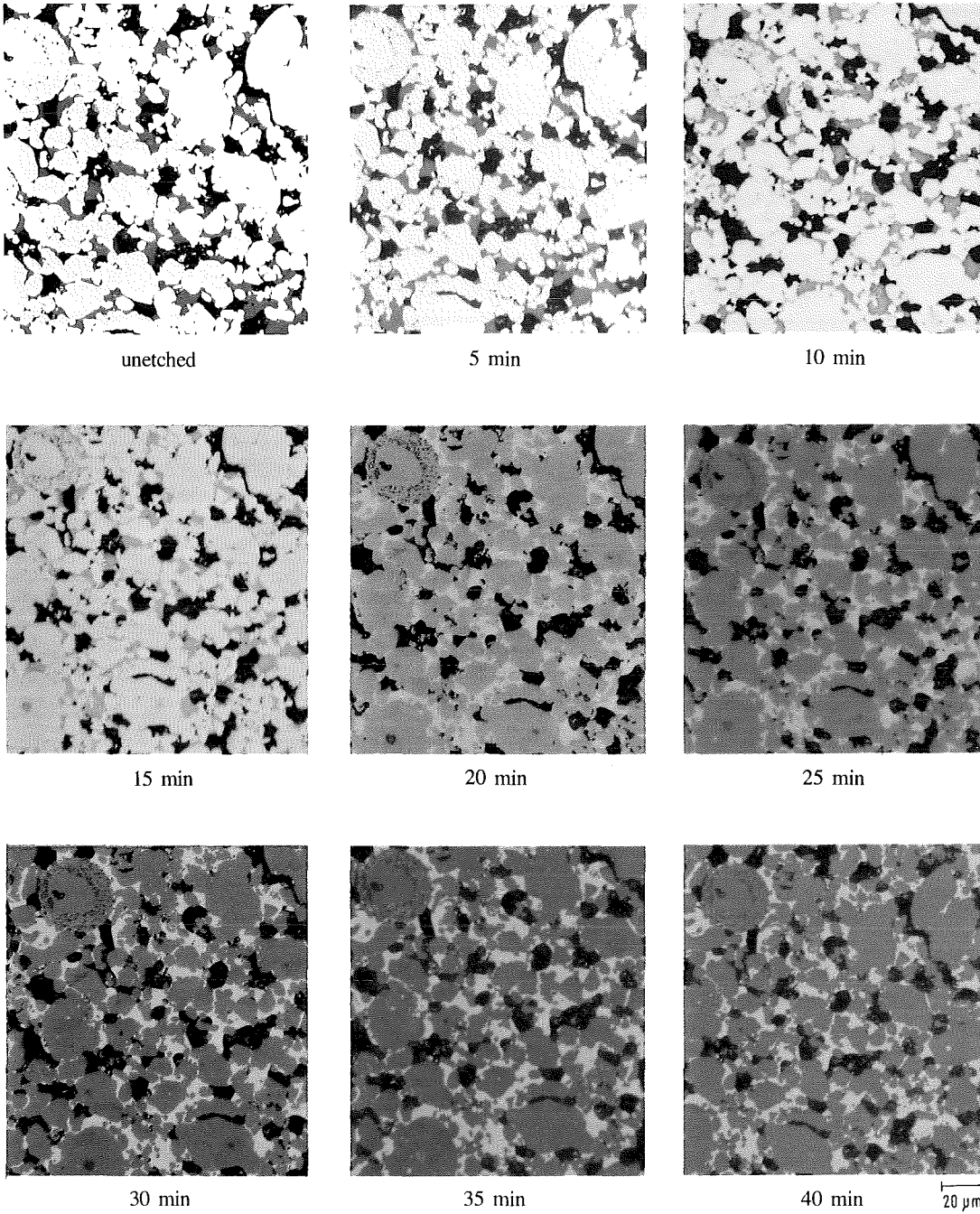
Fig. 5-10. Gas-contrasted porous iron-glass microstructures: pores, black; glass, grey; iron, white when unetched (oxygen as contrasting gas; steel cathode; 0.9 KV).

0 min   20 min   25 min   35 min   50 µm
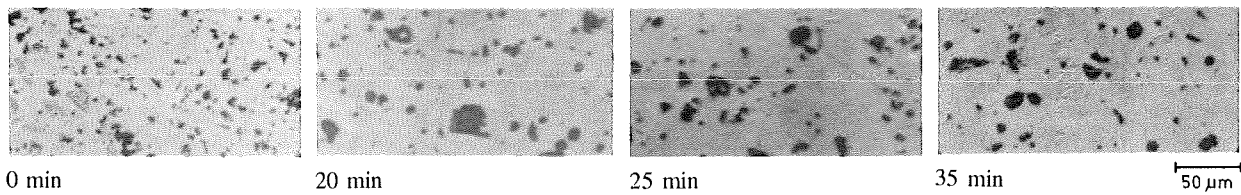
Figure 5-11. Gas-contrasted porous Al_2O_3–ceramic (carbon dioxide as contrasting gas; steel cathode; 1.5kV)
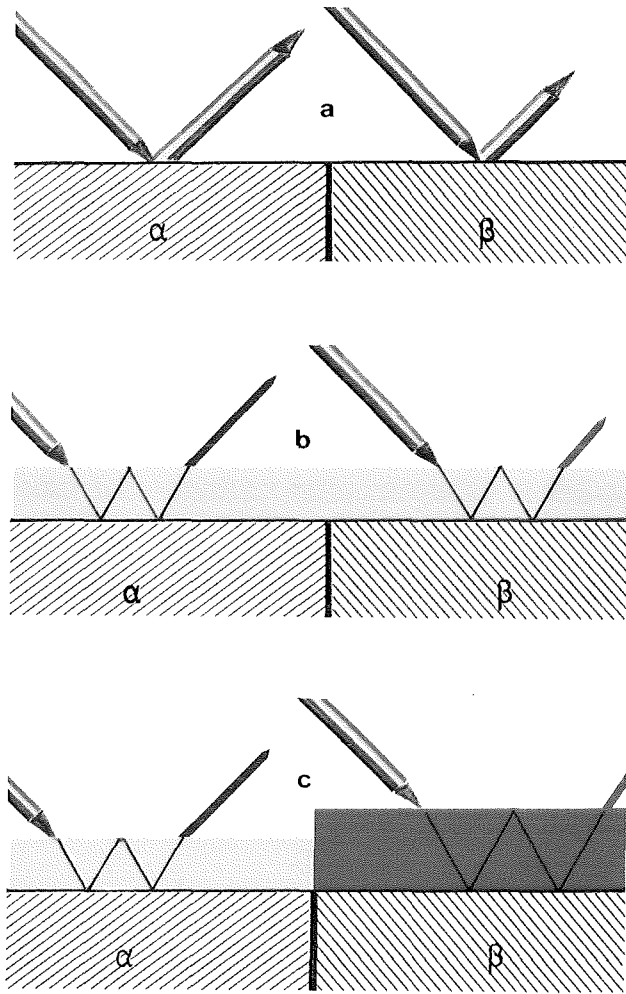
Fig. 5-12. White-light reflection on different phases, α and β : (a) without and (b) with layers of constant, and (c) with different thicknesses.
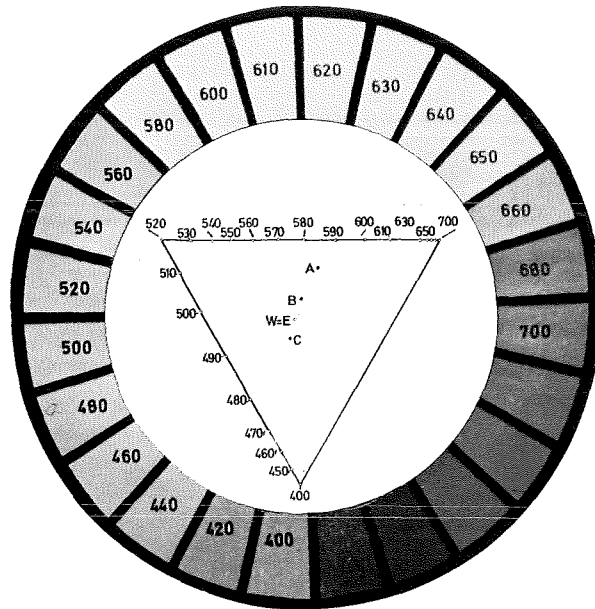
Fig. 5-14. Simplified color chart after Maxwell-Newton-Ostwald (numbers in nm).

Sonderdruck aus:

Praktische Metallographie | Practical Metallography

Zweisprachig
Deutsch/Englisch

Bilingual
English/German

Untersuchungen zum Aufbau von interferenzfähigen Deckschichten auf gaskontrastiertem HfC-Co-Hartmetall

Investigations about the Structure of Interference Coatings on Gas-Contrasted HfC-Co Hard Metal

EBERHARD NOLD, GERHARD ONDRACEK
(Institut für Material- und Festkörperforschung, Kernforschungszentrum Karlsruhe)

Prof. Dr. rer. nat. Dr. h. c. Dr.-Ing. E. h. Günter Petzow zum 60. Geburtstag gewidmet.

Dedicated to Prof. Günter Petzow on the occasion of his 60th birthday

Einleitung

Um die verschiedenen Bestandteile in einem mehrphasigen Gefüge unterscheiden zu können, muß die Wechselwirkung zwischen der Oberfläche dieser Bestandteile und Lichtwellen einen ausreichenden Kontrast ergeben. Dies ist bei polierten Oberflächen meist nicht der Fall. Ihre spezielle Behandlung mit dem Ziel, Kontrast zu erzeugen oder vorhandenen Kontrast zu erhöhen, ist daher ein wesentlicher Teil der Präparation in der quantitativen Gefügeanalyse[1] [2]. Ein insbesondere für mehrphasige Werkstoffe erfolgreiches Kontrastierungsverfahren ist die Gaskontrastierung[3] [4]. Sie wurde hier zur Präparation eines HfC-Co-Hartmetallgefüges eingesetzt, dessen Deckschichten anschließend augerelektronenspektroskopisch untersucht wurden.

Introduction

In order to differentiate between the various components in a multiphase microstructure the interaction between the surface of these components and light waves must produce adequate contrast. This is not usually the case with polished surfaces. Their special treatment for developing contrast or for increasing existing contrast is therefore an important part of the preparation in quantitative micro-structural analysis[1] [2]. Gas contrasting is a successful contrasting technique, particularly for multiphase materials[3] [4]. It has been used here for the preparation of an HfC-Co hard metal microstructure, the surface coatings of which were subsequently investigated by auger electron spectroscopy.

Gaskontrastierung

Die zu untersuchenden Proben enthielten Hafniumcarbid als Hartstoffphase und Kobalt als Bindephase. Sie wurden geschliffen, poliert und mit folgenden Bedingungen gaskontrastiert:

Gas Contrasting

The specimens under investigation contained hafnium carbide as the hard phase and cobalt as the binding phase. They were ground, polished and gas-contrasted under the following conditions:

Apparatur:	Gasätzkammer[3]
Gas:	Sauerstoff,
	~ Atmosphärendruck
Kathoden:	− Blei
	− Stahl
	− Platin
Temperatur:	~ 300 K
Kontrastierdauer:	10 min
Spannung:	1,05 kV

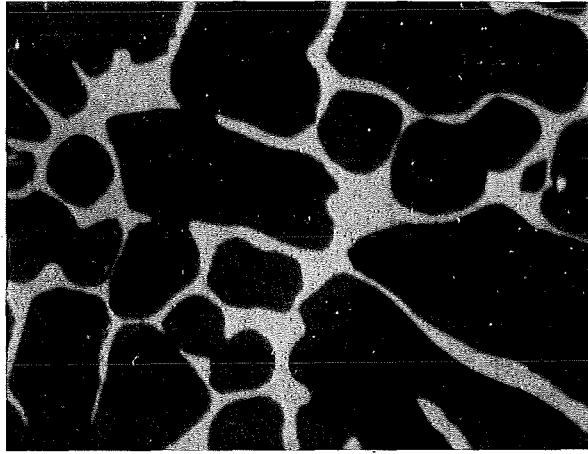| Equipment:	Gas etching chamber[3]
Gas:	Oxygen,
	~ atmospheric pressure
Cathodes:	− Lead
	− Steel
	− Platinum
Temperature:	~ 300 K
Contrasting period:	10 min
Voltage:	1,05 kV

Fig. 1. HfC-Co-Hartmetallgefüge (HfC rot, Co gelb). 500 ×

Fig. 1. HfC-Co hard metal structure (HfC red, Co yellow). 500 ×

Figur 1 zeigt das gaskontrastierte Gefüge, in dem, bei Farbwiedergabe – unabhängig vom gewählten Kathodenmaterial – Kobalt gelb und Hafniumcarbid rot erscheint.

Fig. 1 shows the gas contrasted microstructure in which, in case of colour reproduction, independent of the cathode material selected, the cobalt appeared yellow and the hafnium carbide red.

Schichtuntersuchung

Mit Hilfe der Auger-Elektronenspektroskopie wurden die Deckschichten auf den beiden Phasen separat untersucht. Um unterschiedlich tiefe Lagen der Schichten zu erfassen, wurden diese stufenweise mit Ar-Ionen abgesputtert. Die Versuchsbedingungen wurden bei allen Proben annähernd konstant gehalten:

Spannung	E_P	=	3000 V
Stromstärke	I_P	=	40 μA
Modulationsamplitude	V_{Mod}	=	2 eV
Verstärkerspannung	V_{Mult}	=	1500 V
Zeitkonstante	RC	=	30 ms
Empfindlichkeit	Sens	=	2 mV

Zum Vergleich wurde auch die stoffliche Zusammensetzung der unbeschichteten Oberfläche aufgenommen (Fig. 2), wobei zunächst eine dünne Schicht ($\sim 2 \cdot 10^{-8}$ m) abgesputtert und untersucht, danach wieder abgesputtert ($\sim 10^{-7}$ m) und nochmals untersucht wurde.

In beiden Fällen konnten hauptsächlich die Elemente der Phasen nachgewiesen werden, also Hafnium und Kohlenstoff beim Hartstoff und Kobalt bei der Bindephase.

Investigation of Coating

The coatings on two phases were separately investigated using auger-electron spectroscopy. In order to detect the location of the coatings at different depths they were sputtered off step by step using argon ions. The experimental conditions were maintained approx. constant for all specimens:

Voltage	E_P	=	3000 V
Current intensity	I_P	=	40 μA
Modulation amplitude	V_{Mod}	=	2 eV
Amplifier voltage	V_{Mult}	=	1500 V
Time constant	RC	=	30 ms
Sensitivity	Sens	=	2 mV

For comparison the material composition of the uncoated surface was also recorded (fig. 2). In doing so, a thin coating ($\sim 2 \cdot 10^{-8}$m) was sputtered off and investigated, then sputtered off again ($\sim 10^{-7}$m) and reinvestigated.

In both cases the main elements of the phases were detected, i.e. hafnium and carbon in the case of the carbide phase and cobalt in the case of the binding phase.
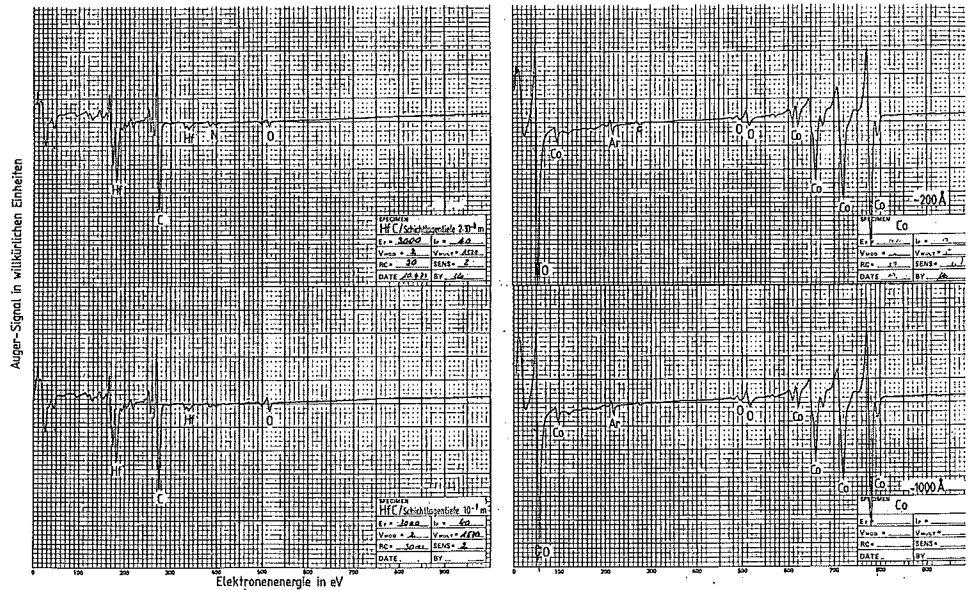
Fig. 2. Auger-Diagramme der unbeschichteten HfC- (links) und Co-Phase (rechts)

Fig. 2. Auger diagrams of uncoated HfC- (left) and Co-phase (right)

Die Ergebnisse der Auger-Analyse der mit Blei-kathode kontrastierten Probe zeigt Fig. 3, diejenigen der mit Stahl- bzw. Platinkathoden kontrastierten Proben sind in Fig. 4 und 5 wiedergegeben.

Zusammenfassend stellt Fig. 6 graphisch dar, daß

– auf der HfC-Phase durch Anlagerung von Sauerstoff und Elementen des Kathodenmaterials an die Oberfläche eine stofflich nicht homogen zusammengesetzte, interferenzfähige Schicht aufwächst, an der die Elemente des Grundmaterials (Hf, C) nicht beteiligt sind.

– auf der Co-Phase durch Anlagerung von Sauerstoff und Elementen des Kathodenmaterials an die Oberfläche ebenfalls eine Schicht aufwächst, an deren Aufbau im Gegensatz zu den Verhältnissen auf der HfC-Phase Kobalt beteiligt ist.

The auger analysis results of the specimen whic had been contrasted with the lead cathode ar shown in fig. 3; figs. 4 and 5 depict those resul obtained for specimens contrasted with ste and platinum cathodes.

Fig. 6 summarizes in graphic form that

– a materially inhomogenously composed ii terference coating develops on the Hf phase as a result of oxygen and elemen comprising the cathode material being dep sited on the surface and that the base mat rial elements (Hf and C) are not present in th coating;

– a coating is likewise formed on the Co phas as a result of oxygen and cathode materi elements being deposited on the surface, ray-structure of which, in contrast to th conditions on the HfC phase, includes coba
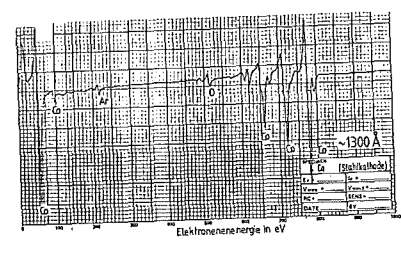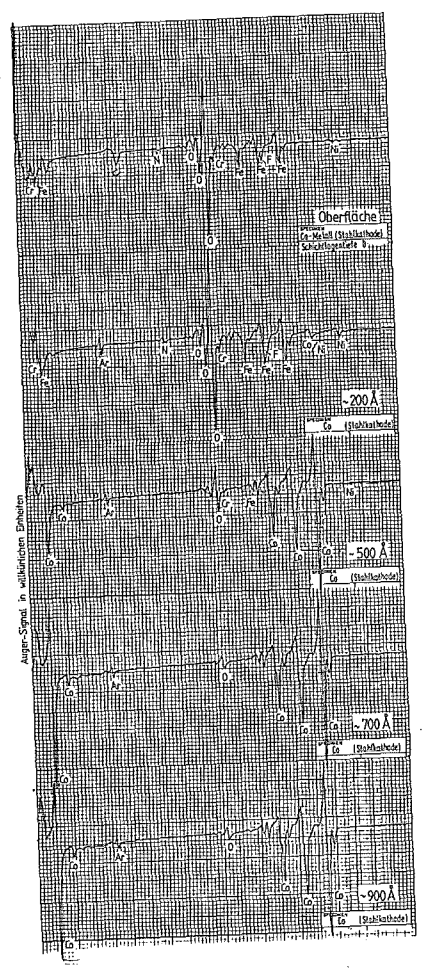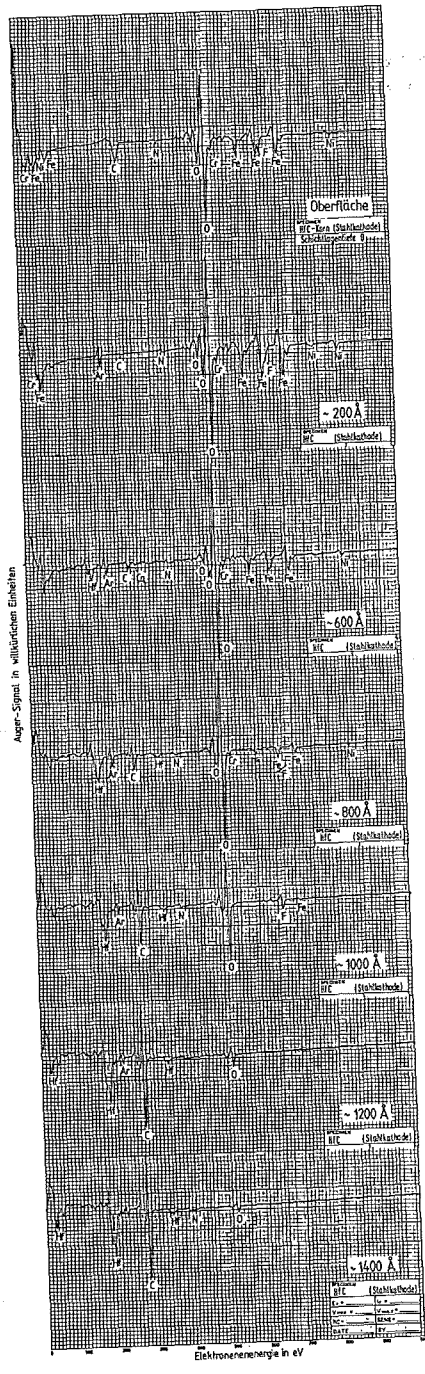
Fig. 3. Auger-Diagramme der beschichteten HfC- (links) und Co-Phase (rechts) nach unterschiedlicher Abtragu der Oberfläche durch Sputtern (Beschichtung mit Blei-Kathode)

Fig. 3. Auger diagrams of coated HfC- (left) and Co-phase (right) after different degrees of surface removal sputtering (coating with lead cathode)
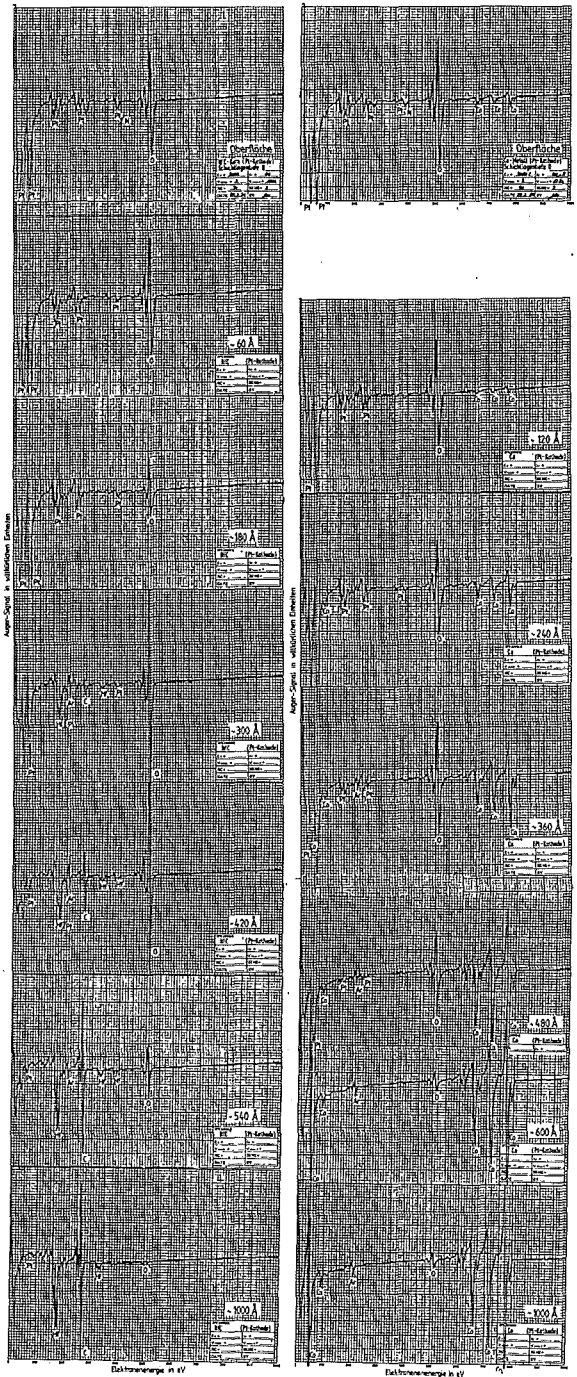
Auger-Signal in willkürlichen Einheiten

Elektronenenergie in eV
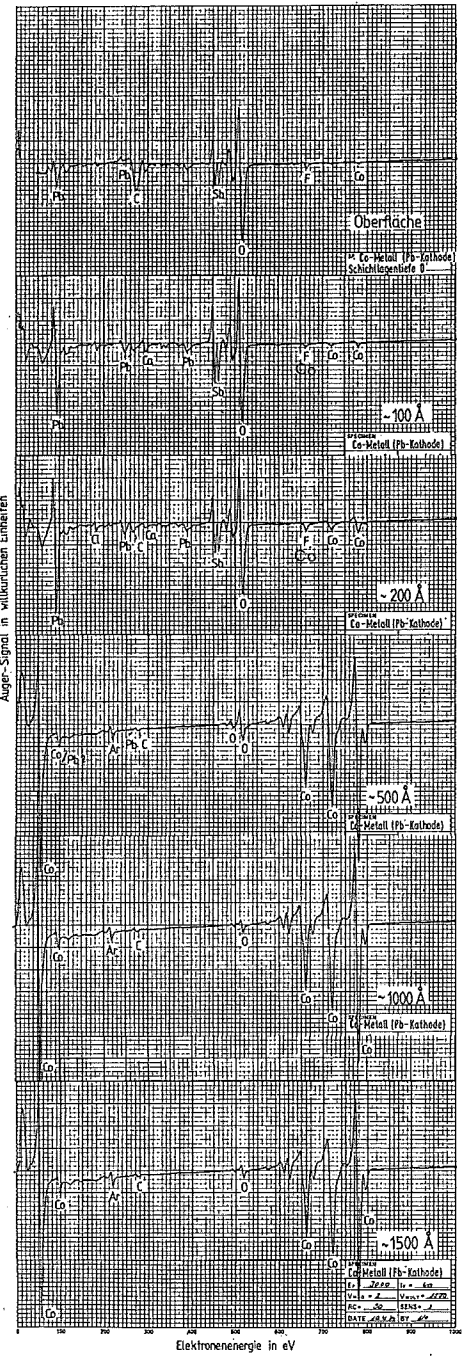
Fig. 4. Auger-Diagramme der beschichteten HfC- (links) und Co-Phase (rechts) nach unterschiedlicher Abtragung der Oberfläche durch Sputtern (Beschichtung mit Stahl-Kathode)

Fig. 4. Auger diagrams of coated HfC- (left) and Co-phase (right) after different degrees of surface removal by sputtering (coating with steel cathode)

Fig. 5. Auger-Diagramme der beschichteten HfC- (links) und Co-Phase (rechts) nach unterschiedlicher Abtragung der Oberfläche durch Sputtern (Beschichtung durch Platin-Kathode)

Fig. 5. Auger diagrams of coated HfC- (left) and Co-phase (right) after different degrees of surface removal by sputtering (coating with platinum cathode)
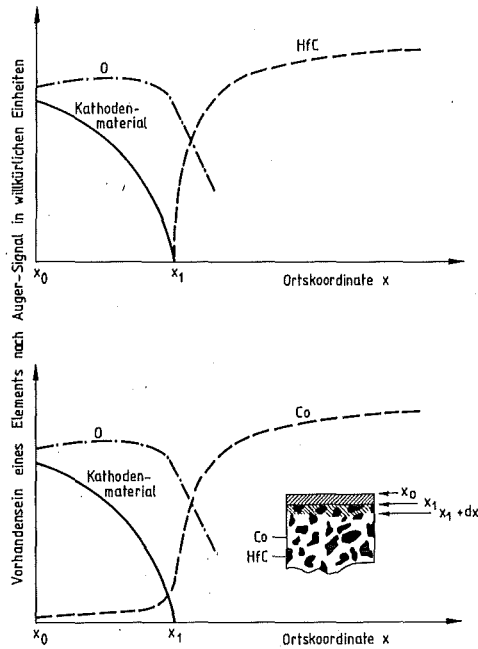
Fig. 6. Qualitative illustration of the composition
coated HfC- (top) and Co-phase surface (bottom)

Die beim Kontrastieren entstehende Schicht be-
steht demnach aus einer aufgewachsenen
Schicht und − möglicherweise − einer Über-
gangszone geringer Dicke und ist auf jeder der
beiden Phasen insgesamt wie auch hinsichtlich
dieser Zonen inhomogen und auf den beiden
Phasen unterschiedlich stofflich zusammenge-
setzt.

The coating formed during contrasting thus co
sists of a developed coating and, possibl
a transition zone of negligible thickness is wi
respect to these zones inhomogenously forme
overall and has a different material compositic
on the two phases.

Ähnliche Ergebnisse wurden bei Untersuchun-
gen von Deckschichten erhalten, die sich bei
chemischer Ätzung bilden[5]).

Similar results were obtained from investig.
tions on coatings which form during chemic
etching[5]).

In Fig. 2 bis 5 sind Näherungstiefen für die
untersuchten Schichtlagen angegeben, die sich
nicht auf Messungen am Probenmaterial selbst
beziehen. Vielmehr wurde bei den Sputterversu-
chen eine Stahlprobe als Standard mitgeführt,
an der unter gleichen Bedingungen die angege-
benen Schichtlagen bzw. die Abtragsrate be-
stimmt wurden.

Approximate depths are given in figs. 2 to 5 f
the coatings under investigations which do n
themselves relate to measurements on the spec
men material. On the contrary, a steel specime
was used as a standard in the sputter expei
ments on which the coatings mentioned and th
removal rate were determined under identic
conditions.

In der Literatur[6]) sind für rostfreien Stahl, Glas
und Aluminium Sputterraten angegeben (2 keV;
Ar^+-Ionenstromdichte 150 $\mu A/cm^2$; Sputterrate
7−13 nm/min), deren Übertragung auf die geo-
metrischen Verhältnisse des vorliegenden Falles
die Extrapolation der Sputterrate erlaubt (2 keV;

Sputter rates for stainless steel, glass ar
aluminium are given in the literature[6]) (2 keV; A
-ion current density 150 $\mu A/cm^2$; sputter ra
7−13 nm/min), which can be transferred to th
geometric conditions of the present case i
permit the extrapolation of the sputter rate

274

Emissionsstrom 30 mA; Argondruck 7 · 10⁻⁸ bar; Sputterrate ~ 5 nm/min).

Um zu überprüfen, ob dieser Richtwert größenordnungsmäßig stimmt, wurde versucht, aus dem durch den Abtrag entstandenen Gewichtsverlust unter Zugrundelegung des mittleren Durchmessers des sichtbaren Sputterflecks und der Dichte des Materials, die Abtragstiefe zu berechnen. Es ergaben sich beispielsweise folgende Vergleichswerte:

keV; emission current 30 mA; argon pressure 7 · 10⁻⁸ bar; sputter rate ~ 5 nm/min).

To check whether this approximate value is of the correct magnitude an attempt was made to calculate the removal depth from the weight loss caused by removal using as a basis the mean diameter of the visible sputter speck and the material density. The following comparative values were obtained by way of example:

	nach Richtwert according to approximate value	über Wägung und Messung by weighing and measuring
Stahl/Steel 14301	2,2 μm	2,2 μm
Stahl/Steel 14988	4,45 μm	4,2 μm
Stellit (Co-Basis)/ Stellite (Co-based)	2,2 μm	2,2 μm

Da die Dicke der zu untersuchenden Schichten auf den Proben um mindestens eine Größenordnung geringer war (< 100 nm) als diejenige für die Vergleichswerte, wurden zusätzlich Schichten bekannter Dicke von Al (60 nm) bzw. Ti (240 nm) auf Glas durch Ar-Ionen abgetragen und die bis zum Erreichen der Glasmatrix erforderlichen Zeiten registriert. Die in der Literatur angegebenen Abtragsraten für Al und Ti wurden bestätigt: Al hat eine ähnliche Abtragsrate wie rostfreier Stahl, die Abtragsrate von Ti ist etwa halb so groß.

As the thickness of the coatings to be investigated was at least a size smaller (< 100 nm) on the specimens than those for the comparative values, coatings of known thickness of Al (60 nm) and Ti (240 nm) on glass were also removed by Ar ions and the times required to the point of obtaining the glass matrix were recorded. The removal rates for Al and Ti given in the literature were confirmed: Al has a removal rate similar to stainless steel and the removal rate of Ti is about half that.

Die in Fig. 2 bis 5 angegebenen Schichtlagentiefen beziehen sich ausschließlich auf diese Stahl- bzw. Al-Standards. Eine direkte Angabe zur Schicht- und Schichtlagendicke auf der HfC- bzw. Co-Phase erlauben sie nicht.

The coating layer depths given in figs. 2 to 5 refer solely to these steel and Al standards. They do not permit a direct statement on the coating thickness and coating layer thickness on the HfC and Co phase.

Zusammenfassung

Das Gefüge eines HfC-Co-Hartmetalls wurde zur quantitativen Gefügeanalyse gaskontrastiert. Dabei bilden sich auf den Gefügebestandteilen interferenzfähige Schichten. Sie verursachen den gewünschten Farbkontrast. Ihr Aufbau wurde in der vorliegenden Arbeit mittels Auger-Elektronenspektroskopie untersucht. Es wurde gefunden, daß unabhängig vom benutzten Kathodenmaterial die Schicht insgesamt hauptsächlich Sauerstoff und das Kathodenelement enthält, daß die Sauerstoffkonzentration ab einer gewissen Tiefe in der Schicht etwa den Wert der unbeschichteten Probe annimmt, daß unter-

Summary

The structure of an HfC-Co hard metal was gascontrasted for the purpose of quantitative microstructural analysis. Interference coatings were formed on the structural components in the process. These produce the desired colour contrast. Their structure is investigated in this work using auger electron spectroscopy. It was found that, independent of the cathode material used, the coating overall contains mainly oxygen and the cathode element, that the oxygen concentration beyond a certain depth in the coating assumes approximately the value of uncoated specimen, that below this depth in the coating

halb dieser Tiefe in der Schicht das Kathoden-
material nicht mehr nachgewiesen werden kann
und daß oberhalb dieser Tiefe in der Schicht auf
der HfC-Phase kein Hafnium oder Kohlenstoff
nachweisbar ist, während auf der Co-Phase Ko-
balt am Schichtaufbau beteiligt ist.

the cathode material can no longer be identified
and that above this depth in the coating no
hafnium or carbon is detectable on the HfC-
phase while cobalt is present in the coating
structure in the Co-phase.

Literatur/References

[1] G. ONDRACEK, Acta Stereol. 1, No. 1 (1982) 5

[2] E. MACHERAUCH, Praktikum in Werkstoffkunde, Vie-
weg (1982) 94

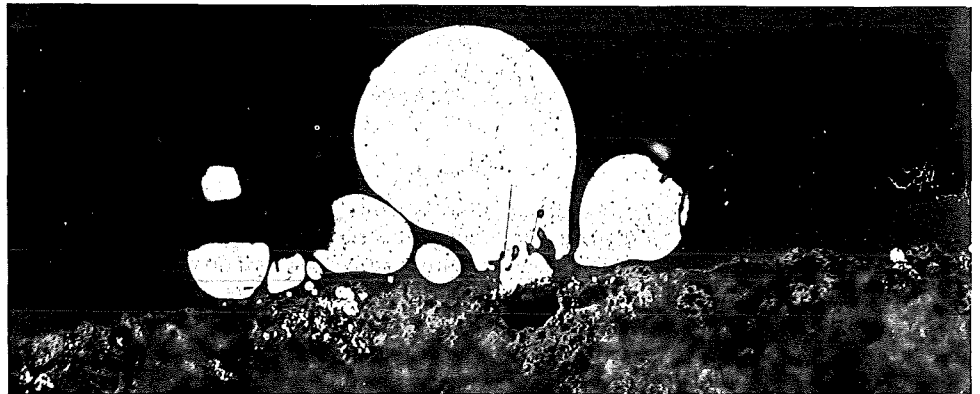[3] G. ONDRACEK, K. SPIELER, Leitz-Mitt. Wiss. Technik
6 (1976) 224

[4] G. ONDRACEK, K. SPIELER, Prakt. Metallographie 1
(1973) 324

[5] H. GAHM, F. JEGLITSCH, E. M. HÖRL, Prakt. Metallc
graphie 19 (1982) 369

[6] A. W. CZANDERNA, Methods of Surface Analysis
Elsevier Sci. Publ. Comp., Amsterdam, Oxford, Nev
York (1975)

Familie Champignon auf dem Sonntagsausflug!
A Mushroom Family on the Way to Their Sunday Picknick
Metalltropfen auf einer Sinterkeramik, ungeätzt. 200 ×
Metal droplets on sintered ceramic, unetched. 200 ×
Aufnahme/micrograph: Erika Bayer, BAYER AG, Krefeld-Uerdingen